Sending-or-Not-Sending with Independent Lasers:
Secure Twin-Field Quantum Key Distribution over 509 km

Jiu-Peng Chen,[1,2] Chi Zhang,[1,2] Yang Liu,[1,2,3] Cong Jiang,[4] Weijun Zhang,[5] Xiao-Long Hu,[4] Jian-Yu Guan,[1,2]
Zong-Wen Yu,[4,6] Hai Xu,[4] Jin Lin,[1,2] Ming-Jun Li,[7] Hao Chen,[7] Hao Li,[5] Lixing You,[5]
Zhen Wang,[5] Xiang-Bin Wang,[2,3,4,*] Qiang Zhang,[1,2,†] and Jian-Wei Pan[1,2,‡]

[1]*Shanghai Branch, National Laboratory for Physical Sciences at Microscale and Department of Modern Physics,
University of Science and Technology of China, Shanghai 201315, People's Republic of China*
[2]*Shanghai Branch, CAS Center for Excellence and Synergetic Innovation Center in Quantum Information and Quantum Physics,
University of Science and Technology of China, Shanghai 201315, People's Republic of China*
[3]*Jinan Institute of Quantum Technology, Jinan, Shandong 250101, People's Republic of China*
[4]*State Key Laboratory of Low Dimensional Quantum Physics, Department of Physics, Tsinghua University,
Beijing 100084, People's Republic of China*
[5]*State Key Laboratory of Functional Materials for Informatics, Shanghai Institute of Microsystem and Information Technology,
Chinese Academy of Sciences, Shanghai 200050, People's Republic of China*
[6]*Data Communication Science and Technology Research Institute, Beijing 100191, People's Republic of China*
[7]*Corning Incorporated, Corning, New York 14831, USA*

Twin-field (TF) quantum key distribution (QKD) promises high key rates over long distances to beat the rate-distance limit. Here, applying the sending-or-not-sending TF QKD protocol, we experimentally demonstrate a secure key distribution that breaks the absolute key-rate limit of repeaterless QKD over a 509-km-long ultralow loss optical fiber. Two independent lasers are used as sources with remote-frequency-locking technique over the 500-km fiber distance. Practical optical fibers are used as the optical path with appropriate noise filtering; and finite-key effects are considered in the key-rate analysis. The secure key rate obtained at 509 km is more than seven times higher than the relative bound of repeaterless QKD for the same detection loss. The achieved secure key rate is also higher than that of a traditional QKD protocol running with a perfect repeaterless QKD device, even for an infinite number of sent pulses. Our result shows that the protocol and technologies applied in this experiment enable TF QKD to achieve a high secure key rate over a long distribution distance, and is therefore practically useful for field implementation of intercity QKD.

Introduction.—Channel loss seems to be the most severe limitation upon practical implementations of long-distance quantum key distribution (QKD) [1–3], given that quantum signals cannot be amplified. Many efforts have been made towards the goal of achieving longer-distance QKD [4–6]. Theoretically, the decoy-state method [7–9] can improve the key rate of coherent-state-based QKD from scaling quadratically to linearly with the channel transmittance, as what behaves of a perfect single-photon source.

Remarkably, under ideal twin-field QKD (TF QKD) [10–17], the secure key rate can be further improved to scale with the square root of the channel transmittance. This TF QKD can also drastically improve the secure distance of QKD. It shows that, the coherent-state source can actually be advantageous over the single-photon source, because it can make use of the linear superposition of the vacuum and one-photon states of the twin field from Alice and Bob. This method has the potential to achieve a key rate that scales with the square root of channel transmittance, and

can by far break the known distance records for existing protocols in practical QKD [5,6]. Although the theoretical secure key rate can be even higher, no key rate of a repeaterless QKD protocol can overcome the Takeoka-Guha-Wilde (TGW) bound [18] and, more tightly, the Pirandola-Laurenza-Ottaviani-Bianchi (PLOB) bound [19], which corresponds to the repeaterless secret key capacity of the lossy channel.

So far, a number of experiments[20–24] for TF QKD have broken the repeaterless QKD bound [19], with [21–24] or without [20] a real fiber, and with [21,24] or without [20,22,23] considering the finite size effect. However, we are still interested in the target of breaking the *absolute limit* of repeaterless QKD. The *absolute limit* here is the unconditional bound value for repeaterless QKD *regardless* of device, including for perfect detection devices. Breaking such a bound is meaningful because we do not have to request any device condition for the repeaterless QKD in comparison. This differs from breaking the relative bound,

which is calculated under the restriction of the actual detection efficiency and about three times lower than the absolute limit. Meanwhile, besides beating the rate-distance limit, chasing a higher key rate and longer distance is itself always another major goal for QKD research. Here, we experimentally demonstrate unconditional breakage of the limit of repeaterless QKD at various distances, and extend the secure distance of QKD to 509 km. In particular, the following properties of our experiment cause it to merit the *unconditional* result in the breakthrough: (1) our setup uses two independent laser sources. There is no incidental light to Alice and Bob, and hence there is no need to monitor the incident light as the implementations directly use seed light from Charlie. In this sense, our experiment maintains measurement-device-independent security. (2) We have taken the finite key effect into consideration with a failure probability of 10^{-10}; this means that the security is based directly upon the final key of the real experiment itself rather than a security on the imagined final key from an infinite number of pulses. (3) Our results break the absolute key rate limit for repeaterless QKD and can be directly deployed in the field.

Since the absolute limit of the key rate is three to four times the relative limit in the prior art experiment [21], we have to fully upgrade our whole system on both theoretical and experimental sides.

First, we adopt the SNS (sending-or-not-sending)-TF-QKD protocol [11] with an improved method for standard two-way classical communication [25,26] with finite size effects [27] being considered. Here, we implement a practical four-intensity method [16] for decoy-state analysis, where each party exploits four different intensities, namely, $0, \mu_1, \mu_2$, and μ_z. To improve the key rate, we take bit error rejection by standard two-way classical communication [25,26] in the post data processing stage. A detailed calculation is presented in the Supplemental Material [28].

Besides optimizing the protocol, we have also substantially improved the experimental setup, as shown in Fig. 1(a). The realization of TF QKD is challenging comparing to other QKD protocols, because precise control of the relative phase from independent lasers through long distance fiber links is required to ensure high quality interference in the measurement station. The phase difference, however, can be accumulated by any wavelength differences between the light sources, or by the fast phase drift in the fiber link [10].

The wavelengths of the two independent lasers are locked with the time-frequency dissemination technology [21], as shown in Fig. 1(b). Alice uses a commercial continuous wave laser source that is internally locked into her cavity, yielding a linewidth under 1 Hz at a 1550.0465 nm central wavelength. Bob locks a stable continuous wave laser source to his cavity using the Pound-Drever-Hall (PDH)
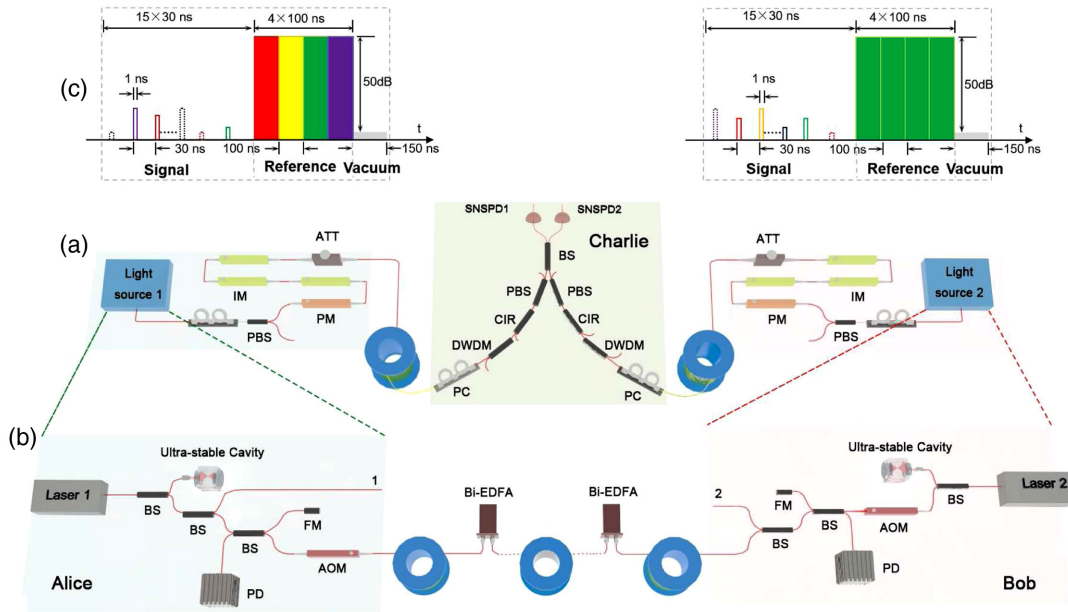

FIG. 1.   (a) Schematic of our experimental setup. Alice and Bob use remotely frequency-locked stable continuous wave (CW) lasers as sources. These light sources are then modulated by a phase modulator (PM) and three intensity modulators (IM1, IM2, IM3) for phase randomization, encoding, and decoy intensity modulation. ATT: attenuator; PC: polarization controller; PBS: polarization beam splitter; DWDM: dense-wavelength-division-multiplexer; CIR: circulator; BS: beam splitter; SNSPD: superconducting nanowire single-photon detector. (b) The remote frequency-locking system for Alice and Bob's light sources. The fiber length is fixed to 500 km for all experimental tests. Bi-EDFA: bidirectional erbium-doped fiber amplifier; BS: beam splitter; AOM: acousto-optic modulator; Bi-EDFA: bidirectional erbium-doped fiber amplifiers; FM: Faraday mirror; PD: photodiode. (c) The time sequence of the basic modulation period. Alice (Bob) sequentially modulates 15 signal pulses, four reference pulses and a vacuum state pulse.

technique [30,31], yielding a linewidth of approximately 1 Hz at a central wavelength of 1550.0474 nm. The frequency difference between the two ultra stable lasers is about 112 MHz, and the relative frequency drift is measured to be approximately 0.1 Hz s^{-1}.

Alice divides her light into two parts, one of which is about 4.1 mW used as her QKD laser source, and the other is about 4 mW sent to Bob as a wavelength reference. Bob receives Alice's reference light and compensates the frequency difference with a feedback bandwidth of approximately 100 Hz using an acoustic-optic modulator (AOM). He then splits his locked light into two parts, one being about 2.3 mW used as his QKD laser source, and the other being about 2.1 mW sent to Alice to compensate the phase noise in the fiber between them with a feedback bandwidth of about 50 Hz. This is done by Alice using an AOM at her output. The response bandwidth of the two AOMs is about 200 kHz, which is fast enough to compensate for the relative frequency and phase drifts between Alice and Bob. The fiber distance between Alice and Bob for this frequency and phase locking is fixed to 500 km in all experimental tests, in order to match the longest distance QKD experiment. The total loss of the 500 km single mode fiber is measured as 98.47 dB. Inserting a Bi-EDFA every 50 kilometers, a total of 9 Bi-EDFAs are used in the path to amplify the signal for frequency and phase locking. The gain of each Bi-EDFA is set to about 11 dB to control the intensity of the signal below the threshold for stimulated Brillouin scattering, and the signal-to-noise ratio of the heterodyne at the photodiode is higher than 40 dB, the whole frequency and phase locking system can work continuously for about one week. We note that this setup can be deployed in field experiments without major changes.

The phase drift in the QKD fiber links is estimated with strong phase reference pulses. In this method, Alice and Bob periodically send such pulses to the measurement station, where the interference result is recorded and analyzed to calculate the relative phase between Alice's and Bob's fibers [21]. We note that, to acquire the phase experienced by the signal pulses, a few requirements must be satisfied. The wavelength of the reference must be set equivalent to that of the signal; reference must transmit along exactly the same optical fiber with the signal. Thus, the phase reference pulses are time-multiplexed with the signal pulses. The intensities of the phase reference pulses are set when enough photons are received at the measurement station. Therefore, the peak intensity in the long distance experiment is high and will inevitably induce additional noise into the measurement besides the detectors' dark counts. This will be discussed in detail later.

In order to avoid the photon number splitting (PNS) [7], unambiguous state discrimination (USD) attacks [32] and to implement phase estimation, the two users individually encode the light into 16 different phase slices using a phase modulator (PM), and into five different intensities using

three intensity modulators (IMs). The highest-intensity pulses are used as references for phase estimation, while the other four are used as the signal, strong decoy, weak decoy, and vacuum state pluses. In order to implement TF QKD over more than 500 km, the intensity ratio between the reference pulses and the vacuum decoy state signal should be higher than 50 dB in the pulse duration. Here, we achieved stable intensity modulation by placing the IMs in a thick foam box to reduce the fluctuations of the ambient temperature and to design a time-multiplexed modulation waveform pattern with different durations and amplitudes between reference and signal pulses. As shown in Fig. 1(c), we set the basic period to 1 μs with a time sequence in which we send 15 signal pulses, each with a 1 ns pulse duration and a 29 ns interval for the first 450 ns; four strong phase reference pulses, each with a 100 ns pulse duration in the next 400 ns; and the vacuum states as the recovery time for the superconducting nanowire single-photon detectors (SNSPDs) in the last 150 ns.

Then we attenuate signals from both sides into a single photon level with passive attenuators. At the measurement station (Charlie), the two beams are interfered at a beam splitter (BS) and the results are detected by two SNSPDs and recorded by a high speed multichannel time tagger. Both the signal and the reference pulses are detected by the SNSPDs, thus, a low dark count rate, high detection efficiency, and high count rate are required simultaneously. We improve the SNSPD by integrating a filter onto the end face of the coupling fiber to reduce the dark count [33] and the insertion loss compared to that in [21]. A series resistor is bonded to the SNSPD chip to accelerate the recovery process and avoid the latching effect. The dark counts of the two SNSPDs are each measured to be both less than 3.5 Hz, with detection efficiencies of 56 and 58%. The maximum counting rates of the detectors are determined to be approximately 10 MHz with continuous light as input.

As mentioned previously, the reflection and scattering of the strong reference pulses will induce various noises. The forward Rayleigh scattering component might be the strongest effect in the long fiber. However, it should not influence the signal because it remains in the same time period as the reference pulses, which are separated by at least 14.5 ns from the signal in the time domain. The same is the case for Brillouin scattering components with small frequency differences, while Raman scattering components are broadband and the chromatic dispersion will move the noise into the signal time span. According to [34], the Raman scattering components are four to six orders of magnitude smaller in intensity than the Rayleigh scattering component and separated from the pump photons frequency by about 13 THz. We tested the Raman scattering noise of about 100 cps at 250 km with an intensity of 12.65 nW for the phase reference pulses, which will increase with a larger pulse intensity. Then we inserted a 100 GHz dense-wavelength-division-multiplexing (DWDM)

filter to eliminate this noise. This still leaves a few noise sources beside the detector's dark count: the reflection of SNSPD or the backward Rayleigh scattering will again introduce backward Rayleigh scattering noise that transmits in the same direction as the signal and distributes uniformly in time domain. The scattering noise from the reflection of SNSPD is about 100 cps and can be removed by inserting a circulator before the SNSPD. The double Rayleigh back-scattering noise is, however, inevitable in our experiment.

Here, we model the total detection noise with double Rayleigh backscattering by

$$d = \frac{P_0 S^2}{4 E_\nu \alpha} e^{-\alpha l} \left[l + \frac{e^{-2\alpha l}}{2\alpha} - \frac{1}{2\alpha} \right] + D_c, \qquad (1)$$

where d is the detection noise count, $S = [2\alpha P_B / P_0 (1 - e^{-2\alpha l})]$ is backward Rayleigh scattering coefficient in fiber, α is the loss coefficient of fiber, P_0 is average intensity of incident light, P_B is the intensity of backward Rayleigh scattering, E_ν is the photon energy, l is the fiber length, and D_c is the dark count of SNSPD. See the Supplemental Material [28] for details on Eq. (1). First, we tested the coefficient of backward Rayleigh scattering using the equation of $S = (2\alpha P_B / P_0)$ in the ultralow loss fiber to estimate the detection noise based on Eq. (1). Then we measured the detection noise in our experiment, as shown in Fig. 2, and found it to agree with the theoretical calculation results and to increase with distance as double Rayleigh backscattering noise comes to predominate. This noise is at the same level as the SNSPD dark counts and is acceptable at 500 km scale.

After all of these upgrades, we performed SNS-TF-QKD over a distance of 509 km ultra-low-loss optical fiber with a channel loss of 84.6 dB and a component loss of 6.2 dB at Charlie. In addition, we performed SNS-TF-QKD over 350 km standard optical fiber and 408 km ultra-low-loss optical fiber. All of the corresponding detailed parameters, including the insertion loss of the fiber links, the optical efficiencies of the optical components at the measurement site, and the proportions and intensities of each state for each fiber length are summarized in the Supplemental Material [28]. To keep the interference stable, we manually calibrated the polarization and fiber delay each hour in the experiment over 350 km and each 45-minute period in the experiments over 408 and 509 km.

Considering the finite data size effect, the secure key rate is calculated [25,26]. Figure 3 shows that the secure key rate at a total distance of 509 km is $R = 6.19 \times 10^{-9}$, with 1.093×10^{12} total pulses sent, and 9.01×10^5 valid detections collected. This key rate breaks the relative bound ($R = 8 \times 10^{-10}$) for the same detection loss by seven times and the absolute linear bound ($R = 4 \times 10^{-9}$) by 1.5 times of repeaterless QKD. Note that the total pulses sent include the decoy and signal state pulses, and that the valid detections are counted in a time window when one and only one of the two detectors clicks. This secure key rate is
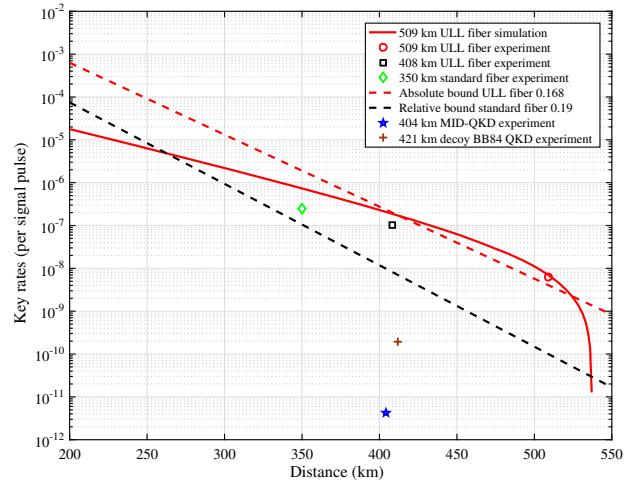
FIG. 3. SNS-TF-QKD secure key rates. The green diamond indicates a secure key rate of $R = 2.42 \times 10^{-7}$ with 2.05×10^{11} total pulses sent and 2.04×10^6 valid detections over a 350 km standard single mode fiber; the black square indicates a secure key rate of $R = 1.03 \times 10^{-7}$ with 3.54×10^{11} total pulses sent and 2.55×10^6 valid detections in the experiment of a 408 km ultralow loss fiber; the red circle indicates the experimental secure key rate over a 509-km ultralow loss fiber. The brown cross indicates the experimental secure key rate of [6], and the blue star point shows the experimental secure key rate of [5]. The red curve shows the simulation result for an ultralow loss fiber length of 509 km with noise probability of 1×10^{-8} and an X-basis baseline error of 0.04; the black dashed curve shows the absolute key rate limit (PLOB bound [19]) of the repeaterless key rate in ultralow loss fiber; and the red dashed curve illustrates the relative PLOB bound [19] of standard optical fiber.
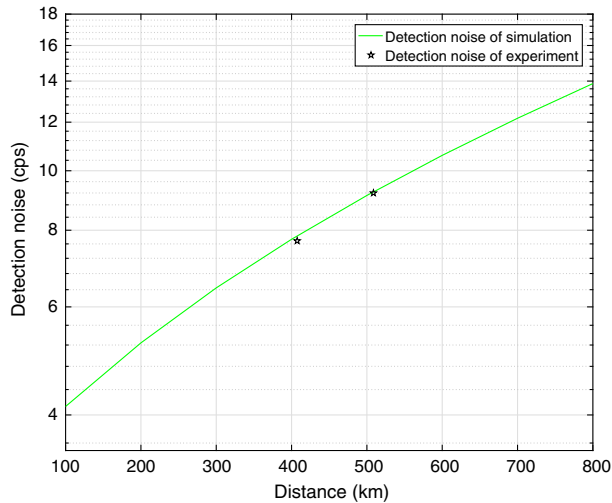

FIG. 2. Theoretical and experimental noise rates with different fiber lengths. Alice and Bob are assumed to emit at the working intensity, with 2 MHz reference counts detected. The green curve shows the theoretical simulation. The black stars are the experimental results.

higher than the absolute PLOB bound in all of these directions, again verifying the high performance of the SNS-TF-QKD with standard two way classical communication [25,26].

In conclusion, we have developed remote optical frequency-locking technique, experimentally implemented the SNS-TF-QKD protocol with two independent lasers to break the absolute key rate limit of repeaterless QKD over a distance of 509 km, and demonstrated a double Rayleigh backscattering noise model to verify the predominance of the detection noises over long distances. Moreover, the 500-km-long accompanying fiber link for the frequency lock makes our system fit naturally into a field test, which will be the next step of this research.

Another interesting question for future research is how to approach the limit of TF QKD. Currently, the dominate noise is the double Rayleigh backscattering noise within the fiber, which is inevitable in our design. One possible solution is to exploit an optical frequency comb instead of a single frequency laser source. The optical frequency comb can simultaneously emit multiple different single frequency lasers while maintaining stable phase differences between each [35,36]. This characteristic of the optical frequency comb is expected to achieve a different wavelength modulation of the reference pulses and the signal pulses in SNS-TF-QKD to avoid the double Rayleigh backscattering noise.

---

[*] xbwang@mail.tsinghua.edu.cn

[†] qiangzh@ustc.edu.cn

[‡] pan@ustc.edu.cn

[1] N. Gisin, G. Ribordy, W. Tittel, and H. Zbinden, Rev. Mod. Phys. **74**, 145 (2002).

[2] V. Scarani, H. Bechmann-Pasquinucci, N. J. Cerf, M. Dušek, N. Lütkenhaus, and M. Peev, Rev. Mod. Phys. **81**, 1301 (2009).

[3] Q. Zhang, F. Xu, Y.-A. Chen, C.-Z. Peng, and J.-W. Pan, Opt. Express **26**, 24260 (2018).

[4] S.-K. Liao, W.-Q. Cai, W.-Y. Liu, L. Zhang, Y. Li, J.-G. Ren, J. Yin, Q. Shen, Y. Cao, Z.-P. Li *et al.*, Nature (London) **549**, 43 (2017).

[5] H.-L. Yin, T.-Y. Chen, Z.-W. Yu, H. Liu, L.-X. You, Y.-H. Zhou, S.-J. Chen, Y. Mao, M.-Q. Huang, W.-J. Zhang *et al.*, Phys. Rev. Lett. **117**, 190501 (2016).

[6] A. Boaron, G. Boso, D. Rusca, C. Vulliez, C. Autebert, M. Caloz, M. Perrenoud, G. Gras, F. Bussières, M.-J. Li *et al.*, Phys. Rev. Lett. **121**, 190502 (2018).

[7] W.-Y. Hwang, Phys. Rev. Lett. **91**, 057901 (2003).

[8] X.-B. Wang, Phys. Rev. Lett. **94**, 230503 (2005).

[9] H.-K. Lo, X. Ma, and K. Chen, Phys. Rev. Lett. **94**, 230504 (2005).

[10] M. Lucamarini, Z. Yuan, J. Dynes, and A. Shields, Nature (London) **557**, 400 (2018).

[11] X.-B. Wang, Z.-W. Yu, and X.-L. Hu, Phys. Rev. A **98**, 062323 (2018).

[12] X. Ma, P. Zeng, and H. Zhou, Phys. Rev. X **8**, 031043 (2018).

[13] K. Tamaki, H.-K. Lo, W. Wang, and M. Lucamarini, arXiv:1805.05511.

[14] C. Cui, Z.-Q. Yin, R. Wang, W. Chen, S. Wang, G.-C. Guo, and Z.-F. Han, Phys. Rev. Applied **11**, 034053 (2019).

[15] M. Curty, K. Azuma, and H.-K. Lo, npj Quantum Inf. **5**, 64 (2019).

[16] Z.-W. Yu, X.-L. Hu, C. Jiang, H. Xu, and X.-B. Wang, Sci. Rep. **9**, 3080 (2019).

[17] J. Lin and N. Lütkenhaus, Phys. Rev. A **98**, 042332 (2018).

[18] M. Takeoka, S. Guha, and M. M. Wilde, Nat. Commun. **5**, 5235 (2014).

[19] S. Pirandola, R. Laurenza, C. Ottaviani, and L. Banchi, Nat. Commun. **8**, 15043 (2017).

[20] M. Minder, M. Pittaluga, G. Roberts, M. Lucamarini, J. Dynes, Z. Yuan, and A. Shields, Nat. Photonics **13**, 334 (2019).

[21] Y. Liu, Z.-W. Yu, W. Zhang, J.-Y. Guan, J.-P. Chen, C. Zhang, X.-L. Hu, H. Li, C. Jiang, J. Lin, T.-Y. Chen, L. You, Z. Wang, X.-B. Wang, Q. Zhang, and J.-W. Pan, Phys. Rev. Lett. **123**, 100505 (2019).

[22] S. Wang, D.-Y. He, Z.-Q. Yin, F.-Y. Lu, C.-H. Cui, W. Chen, Z. Zhou, G.-C. Guo, and Z.-F. Han, Phys. Rev. X **9**, 021046 (2019).

[23] X.-Q. Zhong, J.-Y. Hu, M. Curty, L. Qian, and H.-K. Lo, Phys. Rev. Lett. **123**, 100506 (2019).

[24] X.-T. Fang, P. Zeng, H. Liu, M. Zou, W. Wu, Y.-L. Tang, Y.-J. Sheng, Y. Xiang, W. Zhang, H. Li, Z. Wang, L. You, M.-J. Li, H. Chen, Y.-A. Chen, Q. Zhang, C.-Z. Peng, X. Ma, T.-Y. Chen, and J.-W. Pan, arXiv:1908.01271.

[25] H. F. Chau, Phys. Rev. A **66**, 060302(R) (2002).

[26] H. Xu, Z.-W. Yu, C. Jiang, X.-L. Hu, and X.-B. Wang, arXiv:1904.06331.

[27] C. Jiang, Z.-W. Yu, X.-L. Hu, and X.-B. Wang, Phys. Rev. Applied **12**, 024061 (2019).

[28] See the Supplemental Material at http://link.aps.org/supplemental/10.1103/PhysRevLett.124.070501 for active odd-parity pairing, which includes [29].

[29] C. Jiang, X.-L. Hu, H. Xu, Z.-W. Yu, and X.-B. Wang, arXiv:1908.05670.

[30] R. Drever, J. L. Hall, F. Kowalski, J. Hough, G. Ford, A. Munley, and H. Ward, Appl. Phys. B **31**, 97 (1983).

[31] R. V. Pound, Rev. Sci. Instrum. **17**, 490 (1946).

[32] M. Dušek, M. Jahma, and N. Lütkenhaus, Phys. Rev. A **62**, 022306 (2000).

[33] W. J. Zhang, X. Y. Yang, H. Li, L. X. You, C. L. Lv, L. Zhang, C. J. Zhang, X. Y. Liu, Z. Wang, and X. M. Xie, Supercond. Sci. Technol. **31**, 035012 (2018).

[34] D. Krohn, T. MacDougall, and A. Mendez, *Fiber Optic Sensors: Fundamentals and Applications* (Society of Photo-Optical Instrumentation Engineers, Bellingham, 2014).

[35] T. Udem, R. Holzwarth, and T. W. Hänsch, Nature (London) **416**, 233 (2002).

[36] R. Holzwarth, T. Udem, T. W. Hänsch, J. C. Knight, W. J. Wadsworth, and P. S. J. Russell, Phys. Rev. Lett. **85**, 2264 (2000).